Applied Catalysis B: Environmental 283 (2021) 119651

Contents lists available at ScienceDirect

Applied Catalysis B: Environmental

journal homepage: www.elsevier.com/locate/apcatb

Periodic open cellular structures (POCS) as enhanced catalyst supports: Optimization of the coating procedure and analysis of mass transport

Riccardo Balzarotti [a], Matteo Ambrosetti [a], Mauro Arnesano [b], Alfredo Anglani [b], Gianpiero Groppi [a], Enrico Tronconi [a,*]

[a] Politecnico di Milano, Dipartimento di Energia, Via Lambruschini 4, 20156 Milano, Italy
[b] Dipartimento di Ingegneria dell'Innovazione, Università del Salento, Via per Morteroni, 73100 Lecce, Italy

ARTICLE INFO

Keywords:
POCS
Washcoating
Catalyst deposition
CO oxidation
Mass transfer

ABSTRACT

Aluminum periodic open cellular structures (POCS) of cylindrical shape (9 mm diameter and 4–25 mm length) manufactured by investment casting were investigated as potential enhanced catalyst carriers. Samples with an ideal cubic cell geometry and different cell sizes - namely 1.5, 1.75 and 2.25 mm - were tested. First, coating experiments were performed aiming at understanding the wet coating deposition process: the influence operative spin coating parameters (i.e. spinning speed, time, acceleration) on final coating thickness was studied using glycerol solutions of different viscosity. Based on this preliminary investigation, POCS were activated by depositing a Pd/CeO_2 catalyst by slurry coating techniques and tested under mass-transfer limited conditions in CO oxidation, used as a test reaction for gas/solid limited heterogeneous processes. A correlation for mass transfer performances of these structures in function of the Reynolds number is herein presented and used to compare these novel materials against conventional catalyst supports.

1. Introduction

In recent years, the development of structured catalysts has been widely investigated as a promising approach to improve the overall performance of many processes. Among others, environmental catalysis could draw significative benefits from the adoption of structured catalyst and reactors [1,2]: methane combustion and $deNO_x$ are only few examples of processes that could get remarkable benefits from the application of structured catalysts.

More in general, in industrial research a large variety of supports have been reported in literature, such as honeycomb monoliths, open cell foams, wire mesh and felts [3] that, in specific applications, can overcome the limitations of conventional packed bed reactors such as poor heat and mass transfer and high pressure drops. In this regard, in the last decade open cell foams were widely investigated as potential alternative catalyst supports, especially for processes that suffer from gas/solid heat transfer limitations [4] or external mass transfer limitations like exhaust gas after-treatment applications [5], where the optimal tradeoff between pressure drops and mass transfer is crucial [6]. Metallic supports offer a viable alternative to packed bed reactors also for processes where the heat supply and/or management is critical; as an example it has been documented that thermally conductive open cell foams could represent an optimal solution both for methanol synthesis [7], Fisher-Tropsch synthesis [8], methane steam reforming [9] and water gas shift [10].

A key aspect for the profitability of these structures as enhanced structured supports is their catalytic activation. Several methods have been reported in the literature for catalytic activation of structured substrates via deposition of the active phase, including electrodeposition [2,11], solution-combustion synthesis [12,13] or washcoating [14]. The latter method is widely considered the best compromise between cost, time and results. In a typical procedure, a slurry of the active phase precursor is produced and deposited onto the surface of the structured support by dip-coating [14,15]. In order to remove the slurry entrapped

List of abbreviations: BET, Brauner-Emmett-Teller; CFD, computational fluid dynamics; CPSI, Channels per Square Inch; HC, honeycomb; Mils, 1/1000 of an inch; OFA, Open Frontal Area; POCS, periodic open cellular structures; PVA, polyVynilAlchool; Rpm, revolutions per minute; SEBM, Selective Electron Beam Melting; SEM-EDX, Scanning Electronic Microscopy - Energy Dispersive X-ray Analysis; SLM, Selective Laser Melting; STP, Standard Temperature and Pressure; TCD, thermal conductivity detector.

* Corresponding author.
E-mail address: enrico.tronconi@polimi.it (E. Tronconi).

https://doi.org/10.1016/j.apcatb.2020.119651
Received 18 May 2020; Received in revised form 15 October 2020; Accepted 17 October 2020
Available online 23 October 2020

in the support porosity, a proper driving-force needs to be applied (i.e. gas blowing). Recently, spin coating has been reported in the literature as a valuable technique for the activation of substrates with complex geometry (i.e. open cell foams and monoliths), because the centrifugal force applied to the sample favors the drainage of the excess slurry, hence resulting in a homogeneously thick layer of active material [16, 17].

In view of the needs of process intensification, recently great attention has been devoted to periodic open cellular supports, which can offer higher design flexibility over foams. One of the key features of these supports is the potential to optimize the structure towards higher heat transfer rates [18] or a better tradeoff between mass transfer and pressure drop [19], which are crucial issues for substrates for after-treatment applications.

Klummp et al. [20] studied pressure drops in cubic cell POCS printed with Selective Electron Beam Melting technique (SEBM) in Ti-6Al-V4 from powders with diameters in the 45−105 μm range; structures with different cell sizes, porosities and tilt angle were investigated, showing better performances with respect to random open cell foams in terms of pressure drops. Knorr et al. [21] reported the preparation of structured supports with the same technique, which were coated with microporous carbon and then impregnated with Pd for the catalytic hydrogenation of ethane. These structures have been also tested for several gas/liquid applications in order to optimize the structures towards mass transfer [22,23]. Hutter et al. [24] investigated heat transfer and flow regimes in 3D printed architectures for liquid flows. Al Ketan et al. [25] proposed 3D printed supports with different geometries as an alternative for catalyst carriers in after-treatment devices because of their favorable surface to volume ratio and high porosities, but did not provide any experimental or numerical evidence of their claims. Papetti et al. [19] reported the catalytic activation and testing, alongside with CFD simulations of these structures for after-treatment applications with promising results in terms of -tradeoff between conversion and pressure drop.

Manufacturing of these structures by means of 3D printing still represents a challenge both in terms of the combined dimensional accuracy and the small geometries required in many of the catalytic supports in order to maximize the specific surface area [26]. Other concerns are related to the surface finishing of the sample, that, in the case of metal 3D printing, results in a residual roughness in the range of the dimension of the starting powder. One of the biggest issues is still how to make possible the large-scale production of these materials.

In this regard, conventional investment casting manufacturing may combine the requirements to produce such novel engineering materials with a conventional manufacturing technique that has been already on the market for several decades. Parametric studies revealed that with this method structures with porosities up to 93 % and struts with diameters in the 0.4−1 mm range can be easily manufactured [26].

Despite the remarkable interest in these supports, at the present time only limited information is present in the literature regarding their catalytic activation; in particular, a detailed rationalization of the washcoating procedures that are needed to generate catalytically active supports is missing. In this view, the aim of the present work is to fill this gap by providing a complete overview of the application of spin coating techniques to these supports, analyzing the influence of support morphology (i.e. cell size, porosity, sample length) and operative conditions (i.e. liquid media viscosity, spinning velocity, acceleration and time) on wet coating deposition by using model liquid solutions based on water-glycerol solutions. According to the preliminary conclusions from these tests, POCS supports were catalytically activated by slurry coating technique, depositing a thin Pd/CeO_2 washcoat layer onto support surface. Catalytic performances in CO oxidation were then evaluated and compared with results already collected for open-cell foams aiming to derive a new correlation able to describe the gas/solid mass transfer properties of these structures in function of their geometrical properties. On the basis of this analysis, we performed a comparison of volumetric mass transfer rates that can be obtained with these structures and with square channel honeycombs. Mass transfer rates of the tested structures are quite low with respect to industrial honeycombs, showing that further developments of 3D printed techniques are needed to enable the design of supports with smaller strut and cell sizes to increase the surface area of the support and consequently the mass transfer rates.

2. Experimental

2.1. Catalyst preparation and characterization

The CeO_2 catalyst carrier was produced by precipitation. In the experimental procedure, cerium nitrate ($Ce(NO_3)_36H_2O$, Sigma-Aldrich) was used as a precursor, while ammonium carbonate ($(NH_4)_2CO_3$, Sigma-Aldrich) was used as precipitating agent. Both salts were dissolved in distilled water to obtain 1 M and 2.6 M solutions, respectively. Ammonium carbonate solution was added to cerium nitrate solution at room temperature under magnetic stirring. The resulting slurry was filtered and washed with distilled water to reach neutral pH. After drying overnight at 120 °C, the powder was calcined at 500 °C for 3 h (heating and cooling rates set at 2 °C min^{-1}). Thus, high surface area cerium oxide (in the following labelled as CeHS) was obtained [27].

Cerium oxide powders were catalytically activated by the incipient wetness technique [28]. Palladium nitrate ($Pd(NO_3)_2$ (12–16 % w/w aqueous solution from Alfa Aesar) was used as precursor of the metal active phase. Pd content was fixed at 3 % wt. with respect to metal and carrier total mass, while the total solution volume was calculated according to the specific pore volume of the carrier. After impregnation, the powders were dried overnight at 120 °C and, then, calcined at 500 °C for 10 h (heating and cooling rate set at 2 °C min^{-1}). The calcination temperature was suitable for both slurry organic components decomposition and palladium nitrate oxidation to PdO. In the following, the catalytic powder will be identified as PdCeHS.

Metal active phase content was quantified by SEM-EDX measurements; an EVO 50 Series Instrument by ZEISS equipped with an INCAEnergy 350 EDS micro analysis system and an INCASmartMap for imaging the spatial variation of elements in the sample were used.

Thermogravimetric analyses were performed using an Extar 6000 instrument by Seiko Instrument. According to a procedure reported in [29], two heating-cooling cycles between room temperature and 1000 °C were run in air (5 °C min^{-1} for both heating and cooling steps).

N_2 adsorption and Hg intrusion techniques were used to determine BET surface area and pore volume, respectively, using a Micromeritics Tristar 3000 instrument. Values of 90 m^2 g^{-1} and 0.52 mL· cm^{-3} were found for surface area and pore volume, respectively.

2.2. Washcoat deposition and characterization

POCS (produced and supplied by Department of “Ingegneria dell’Innovazione”, University of Salento [26]) were used as structured supports. Fig. 1 shows an image of the POCS unit cell, a 3D rendering of the samples and a picture of the structures with different d_{cell}.

Different open cell sizes were tested, namely 1.5, 1.75 and 2.25 mm, while the strut thickness was held constant at 0.5 mm; the latter represents the current limitation in terms of minimum size of ligaments that can be produced. The cell size of the samples was chosen in order to obtain structures with porosities in the range 0.7−0.93, to mimic typical values of foams and monoliths. Supports were designed in a form of cylinders with an external diameter equal to 9 mm, equal to the diameter of the reactor to be used for catalytic tests, and an outer skin thickness of 0.5 mm; the length of the catalytically tested supports was set at 20.5 mm for samples with cell sizes of 1.5 mm and 2.25 mm and at 14.5 mm for samples with cell size of 1.75 mm. Additionally, samples with 2, 3, 7, 11 and 14 cells in longitudinal direction and cell size of 1.75 mm were cut from the original samples and used for the

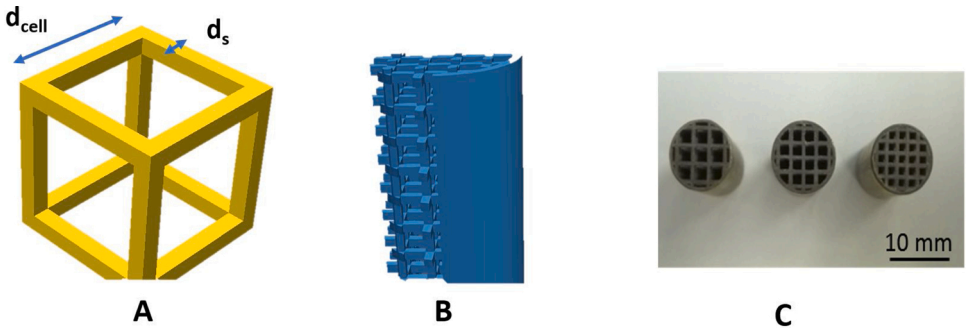

Fig. 1. Schematic representation of the POCS structure : A) unit cell, B) 3D rendering of the samples where a portion of the skin has been removed to show the internal structure, C) top view of the samples used for experimental tests.

investigation of coating deposition. Geometrical features of the samples used in this work are listed in Table 1. Sample I instead was cut from a structure with a higher external diameter by water-jet; this structure is therefore characterized by the absence of the external skin.

2.2.1. Assessment of wet coating deposition on POCS

The influence of spin coating parameters on coating deposition on POCS was investigated by using model liquids. In particular, pure glycerol (in the following labelled as HG [0:100], supplied by Sigma Aldrich, purity >99 %) and water glycerol solutions at different concentrations were used in order to investigate a broad range of liquid viscosities (Table 2).

In order to perform liquid deposition onto POCS structures, a coupled dip coating and spin coating procedure was carried out. On the basis of what reported in a previous work [30], POCS were immersed and withdrawn by hand with no withdrawal speed control, as the washcoat load after spin coating was found to be independent of withdrawal velocity on similar supports. Then, a commercial spin-coater (SPIN 150i spinner by SPS) was used to remove the excess liquid that was entrapped in the support porosity; after spinning, the skin outer surface was cleaned. A specifically designed sample holder was used in order to fix the three-dimensional POCS structure to the spinning shaft [30]. Due to the device modification a maximum of 3000 rpm in rotation speed was set for safety reasons. Spinning time, speed and acceleration were precisely controlled, while the coating deposition was monitored by gravimetric analysis. The deposited coating mass was determined by comparing the weight of the bare POCS with that of the coated sample after spinning. Wet coating mass value was used to calculate the average wet coating thickness, according to Eq. 1:

$$Wet\ coating\ thickness\ = \frac{Wet\ coating\ mass\ [g]/Liquid\ Density\ [gcm^{-3}]}{POCS\ total\ internal\ surface\ area\ [cm^2]} \quad (1)$$

where the wet coating mass (g) is the difference of the weight of the bare POCS from that of the coated POCS after the spinning. By dividing the wet coating mass by the liquid density (g cm^{-3}), the volume of deposited liquid (cm^3) is obtained at the numerator in Eq. 1, if evaporation has not changed the liquid density. This assumption is reasonable for the model coating liquids that were rich in glycerol. Coating thickness (cm) is finally obtained by dividing the wet coating volume (cm^3) by the total internal surface area (cm^2) of the POCS structure, which is calculated as the sum of the area of struts surface and the area of skin internal surface.

Table 1
Geometrical properties of bare POCS. For all samples, support diameter and strut thickness are equal to 9 mm and 0.5 mm, respectively.

Sample name	Cell size [mm]	Sample length [mm]	Number of longitudinal cells	Internal Surface Area [mm^2]	S_v [m^{-1}]	Porosity
A	1.75	4	2	445	1748	0.756
B	1.75	5.75	3	604	1652	0.768
C	1.75	9.75	5	958	1586	0.778
D	1.75	14.5	7	1403	1521	0.781
E	1.75	19.5	11	1889	1522	0.786
F	1.75	25	14	2361	1485	0.791
G	1.5	20.5	16	2668	2046	0.740
H	2.25	20.5	8	1329	1019	0.860
I	3	15	5	n.e.	535	0.930

Table 2
Water (H) and glycerol (G) mixtures used as model liquids: resume of compositions and properties at 25 °C.

Sample name	Water content [% wt.]	Glycerol content [% wt.]	Density [g cm^{-3}]	Viscosity [Pa s]
HG 0–100	–	>99 %	1.26	1.412
HG 5–95	5	95	1.25	0.523
HG 15–85	15	85	1.22	0.109
HG 25–75	25	75	1.19	0.035

2.2.2. Structured support activation

Before coating deposition, POCS were washed with acetone for 30 min in an ultrasonic bath. The supports were catalytically activated by the slurry coating process [31]. Powder slurry was produced according to a procedure reported in literature [15]. The liquid medium, which will be labelled as HGP in the following, is composed by glycerol (G, dispersant), distilled water (H, solvent/diluent) and polyvinyl alcohol (PVA). The latter acts both as rheology modifier and as binder, until its decomposition during flash drying. Components were added with mass ratios of 1.9 w/w, 1.8 w/w and 0.07 w/w with respect to PdCeHS mass, for glycerol, water and PVA, respectively.

In a typical procedure, PVA was dissolved in water at 85 °C under magnetic stirring. Then, glycerol was added under magnetic stirring, after cooling down the water-PVA solution to room temperature. Pd-supported cerium-based powders were mixed with the HGP liquid medium and ball milled for 24 h at 50 rpm using zirconium oxide milling bodies. After milling, ethanol (0.39 w/w with respect to powder mass) was added to the formulation to reduce foaming.

Slurry rheological properties were assessed by means of a dynamic stress device by Rheometrics (DSR 200 device). Parallel disc plates (diameter 40 mm) were used and viscosity was evaluated in the 1-10^3 s^{-1} shear rate range, at 25 °C.

The coating deposition was performed by spin coating. In the experimental procedure samples were manually dipped into the slurry and withdrawn; then, they were spaced in a specifically designed sample holder and spun in order to remove excess slurry. Rotation speed was set at 2000 rpm, while rotation time was set at 10 s. Then, the wet coating layer was flash dried at 350 °C for 6 min in a preheated oven [15]. In order to reach the target catalyst load onto the POCS supports (i.e.

washcoat inventory in the 20–40 $g_{cat} \cdot l^{-1}$), the deposition/flash drying procedure was repeated up to 3 times, depending on the support cell size. Finally, samples were calcined at 500 °C for 10 h, with 2 °C min^{-1} heating and cooling ramps [28].

Washcoat load was assessed by means of gravimetric analysis. Coating layers homogeneity and morphology were evaluated by optical microscopy (SteREO Discovery.V12 equipped with Axiocam ERc 5 s camera, from Zeiss).

Washcoat thickness measurements were performed on samples after fracture analysis. This method has been previously reported as a valuable methodology for determining the average coating thickness of complex geometry substrates [17], as it allows sampling the coating thickness at different height and locations in the support. Samples were included in epoxy resin (E30 by Prochima) in order to prevent deposited layers from detachment. After resin curing, samples were cut and internal faces were accessible. Washcoat layers morphology and thickness were thus qualitatively characterized by optical microscopy (Aristomet microscope by Leica, equipped with DXM1200 F digital camera from Nikon).

2.3. Catalytic tests

Catalytic activity was evaluated for different POCS supports performing CO oxidation in air through a 9 mm tubular lab-scale reactor, placed into an oven as represented in Fig. 2. CO oxidation over Pd/CeO_2 catalyst was chosen as test reaction to monitor mass transfer properties of the samples due to its extremely high activity. The methodology has been already applied to the evaluation of the external mass transfer properties of open-cell foams [6,32]. The samples were loaded in a micro-tubular reactor (internal diameter. 9 mm) placed in an oven. Pieces of bare POCS (1 cm in length) were cut from the original samples for each geometry and placed upstream and downstream the catalytic sample to avoid flow maldistributions. Two temperature measurements were collected; the first one in contact with the inlet bed cross section (Thermocouple 1 in Fig. 2), while the second one at the outlet section of the uncoated support (Thermocouple 2 in Fig. 2).The difference between the outlet and the inlet temperature due to the heat released by the reaction was up to 90 °C.

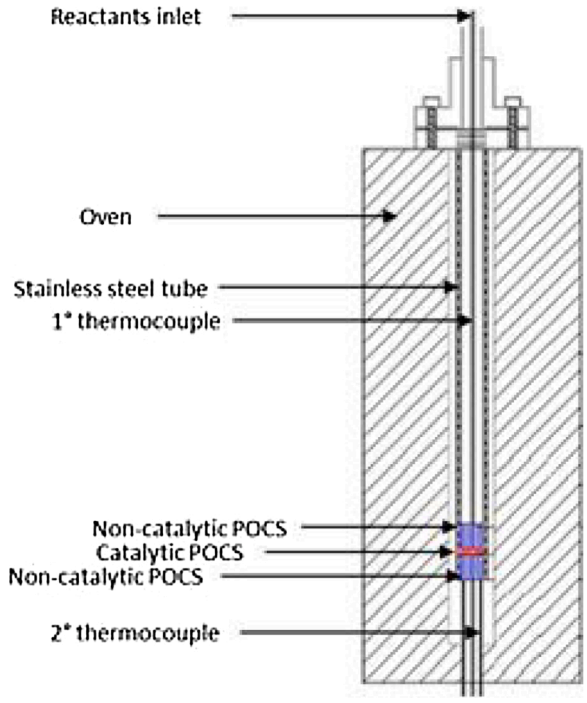

Fig. 2. View of the reactor configuration used for mass transfer tests.

Reactants were fed through independent lines and regulated by mass flow controllers (5850E model by Brooks); before entering the oven, gases were mixed and preheated with an electric coil up to 125 °C.

Over the investigated samples, CO catalytic combustion in air was performed feeding to the reactor flow rates in the range 1000–9000 cm^3 min^{-1} at Standard Pressure and Temperature (STP)[1] using 1.5 % of CO in the feed. With such reactor diameter and flow rates, it was possible to test mass transfer properties of these structures at flow velocities in the range [m s^{-1}, in the operative range of ATS systems. The composition of reactants and products was analyzed with a gas chromatograph (model 6890 N from Agilent Technologies) equipped with two thermal conductivity detectors (TCD) and two packed columns, one filled with Molecular Sieve 5A mesh suitable to analyze O_2, N_2 and CO, the other column filled with Porapak Q 80/100 to separate CO_2. Nitrogen was chosen as reference for the molecular sieves column, while the pseudo-component consisting of a mixture of N_2, O_2 and CO was chosen for the Porapak column.

To enable the investigation of mass transfer at low Reynolds numbers, following the same criteria presented in [33], CO oxidation tests with a strong dilution of helium were performed co-feeding 1.5 % of CO in a mix with 5% of O_2 diluted in helium. The reactant composition was quantified with a micro-GC (GCX model by Pollution) equipped with TCD and two capillary coated columns coated with molecular sieves and Poraplot Q. The mol-sieve column used argon as elutant and reference gas, hence helium was the internal standard, while for the Poraplot column the pseudo-component was the reference for the quantification of CO_2.

In order to collect a complete ignition curve, the temperatures of the oven and of the preheater were increased stepwise; only analyses at steady state were considered, determining the CO conversion as the ratio of the carbon monoxide concentration in the outlet and in the inlet stream. Carbon balances were considered acceptable with an error in the range ± 5%.

Absence of catalytic activity of the reactor and of the bare support was checked, showing CO conversions lower than 5% below 500 °C. The absence of bypass was checked by running tests at low flow rate (1000 cm^3 min^{-1} at STP) and observing an almost complete CO conversion, thus confirming adequate activity of the catalyst and the absence of flow channeling within the tube wall-POCS gap.

3. Results and discussion

3.1. Assessment of spin coating parameters

A preliminary support characterization was performed by calculating the POCS geometrical properties. Results are reported in Table 1. In order to determine the internal surface area, the samples were three-dimensionally reconstructed using open source software (OpenScad) and the total surface area of the POCS was calculated by using the MeshLab software. During the deposition process, only POCS internal surface is relevant for washcoat deposition process, since the external skin surface was cleaned before evaluating the weight increase. For this reason, the internal surface area was calculated as the difference between the total surface area determined by MeshLab and the skin outer surface. The specific surface area (S_v, m^{-1}) was calculated as the ratio of POCS internal surface area to POCS volume.

3.1.1. Influence of spin coating conditions and liquid viscosity

The influence of spin coater angular acceleration was assessed in the 100−2000 rpm s^{-1} range. In these experiments, tests at spinning time equal to zero were performed, in order to focus only on the effects of device acceleration. At each test, deceleration was set at the same value of acceleration. Results are shown in Fig. 3 for 2.25 mm (sample H) and

[1] 298K and 1 bar

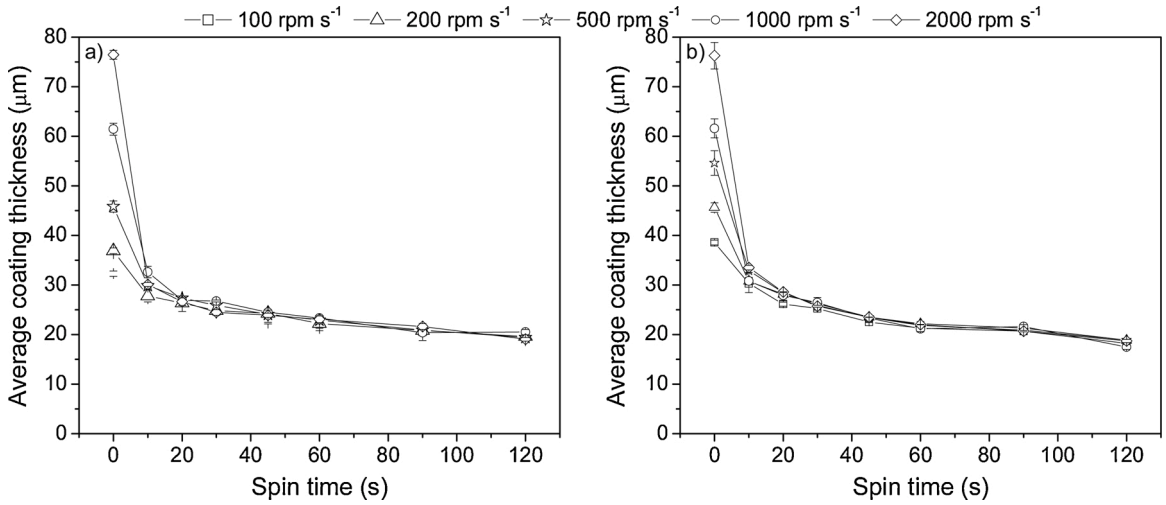

Fig. 3. Influence of acceleration on average wet coating thickness for 2.25 (a) and 1.5 mm (b) cell size POCS using an 85 %wt. glycerol solution. Error bars are the standard deviation from 3 replicate experiments. Steady state spinning speed is set at 2000 rpm.

1.5 mm (sample G) cell size POCS, using a liquid medium with viscosity equal to 0.109 Pa s (i.e. 85 %wt. glycerol solution) and a steady state spinning speed of 2000 rpm.

The experimental points at "0 spinning time" consist in an increase and decrease of speed, at fixed acceleration and deceleration, without any rotation hold at steady state conditions. Due to the different values in acceleration and to the same final spinning speed, each test at "0 spinning time" condition exhibited a different duration. In view of these operative conditions, it is evident that acceleration plays a role in the determination of the washcoat thickness at "0 spinning time" condition: the higher the acceleration, the thicker the average wet coating. This trend may be induced by the difference in rotation time: indeed, at 2000 rpm s^{-1} acceleration, each spinning test lasts only 2 s, which may be not enough to properly remove excess slurry that is entrapped in support porosity. As the spinning time (i.e. the time of the hold at constant spinning rate equal to 2000 rpm) increases, the influence of acceleration becomes weaker and, approximately from spinning time equal to 10–15 seconds, it is almost negligible. Thus, if the rotation time is long enough, acceleration doesn't affect the final coating thickness.

Accordingly, the influence of spinning speed and time on the average coating thickness was assessed (Fig. 4) by testing sample F (i.e. cell size of 1.75 mm and length of 25 mm) with a spinning time ranging from 10 s to 120 s. During these tests, acceleration was kept constant at 1000 rpm s^{-1}.

Average wet coating thickness decreases on increasing both the spinning speed and time (Fig. 4-a), due to the increase of the intensity and the duration of centrifugal forces, respectively. These results are confirmed using a 75 %wt. glycerol solution (Fig. 4-b). Spinning speed also influences the dynamics of the excess liquid removal; indeed, an increase in spinning speed allows reaching a steady-stated condition in shorter times, both with high and low viscosity fluids (Fig. 4-a, pure glycerol with 1.412 Pa s viscosity and Fig. 4-b, 75 %wt. glycerol solution with 0.035 Pa s viscosity). This is probably correlated to an increased shear stress on the fluid at the liquid-solid interface, as spinning speed increases. Thus, the steady-state condition is reached in shorter time, as the driving force for excess liquid removal is higher.

In order to assess the influence of liquid medium viscosity on wet coating load, different water/glycerol solutions were used. Results are reported in Fig. 5.

Liquid media composition (and thus viscosity) affects the thickness of wet coating after spinning treatment. Indeed, viscosity ranged from 1.412 Pa s (pure glycerol) to 0.035 Pa s (75 %wt. glycerol solution), with a variation of 2 orders of magnitude, while the maximum wet coating thickness (26 μm, with pure glycerol) was only twice the minimum one

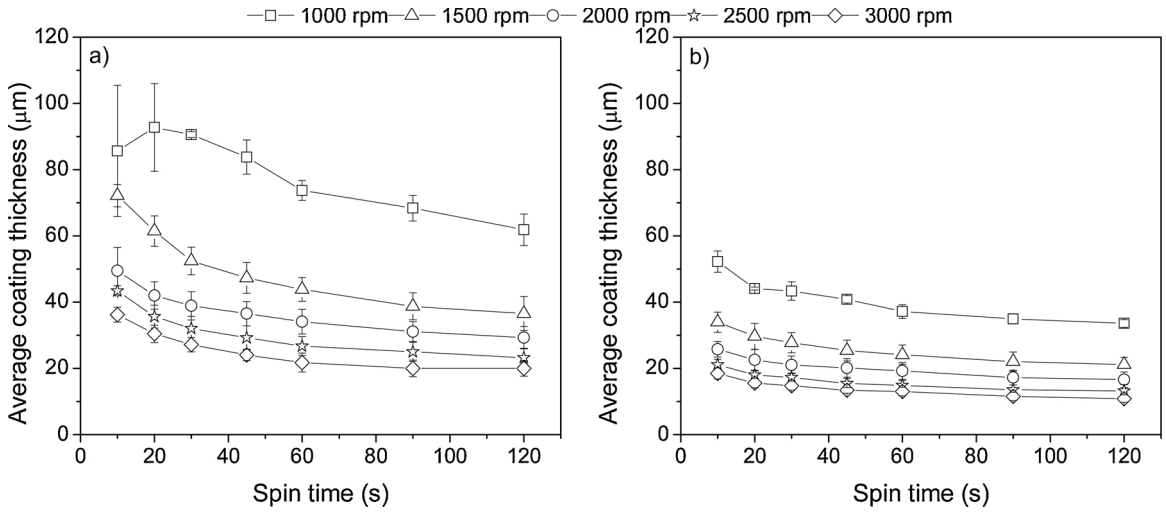

Fig. 4. Average coating thickness as a function of spinning speed and spinning time, using model liquids on sample F POCS (1.75 mm cell size, L =25 mm): pure glycerol (a) and 75 %wt. glycerol solution (b). Error bars are the standard deviation from 3 replicated experiments.

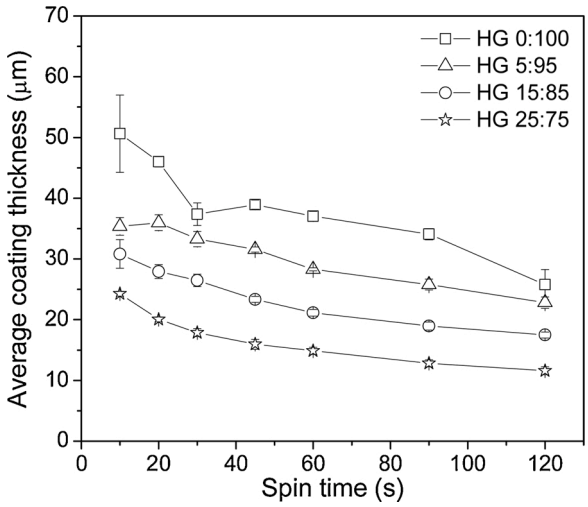

Fig. 5. Influence of viscosity on average wet coating load on POCS with 1.5 mm cell size. Spinning speed is fixed at 2000 rpm. Error bars are the standard deviation from 3 replicate experiments.

(12 μm, with 75 %wt. glycerol solution). At the author's knowledge, neither a phenomenological description of entrained liquid removal nor equations to predict the final average coating thickness are available in literature for the coating deposition onto POCS structures. Reported results evidenced a steady-state thickness dependence to $\eta^{0.25}$, in comparison to $\eta^{0.5}$ for rotating discs [34]. Such difference can be ascribed to the complexity of the three-dimensional structure, as both the internal skin and the struts would play different roles in the process of coating deposition, whose superposition determines the final coating thickness.

3.1.2. *Influence of support characteristics*

In order to completely clarify the coating deposition process onto POCS, the influence of support geometrical characteristics (i.e. support length and cell size) was assessed. For evaluation of the influence of support length, POCS of 4, 5.75, 9.75, 14.5, 19.5 and 25 mm length were tested (Fig. 6). The 9.75 mm POCS was produced by joining two POCS with 5.75 mm and 4 mm length, respectively.

Results regarding the influence of POCS length on wet coating load, at fixed cell dimensions, are presented in Fig. 7. Samples were spun at 2000 rpm for 90 s in order to investigate the steady-state condition of film deposition process.

POCS length was found to play a role on coating thickness, which

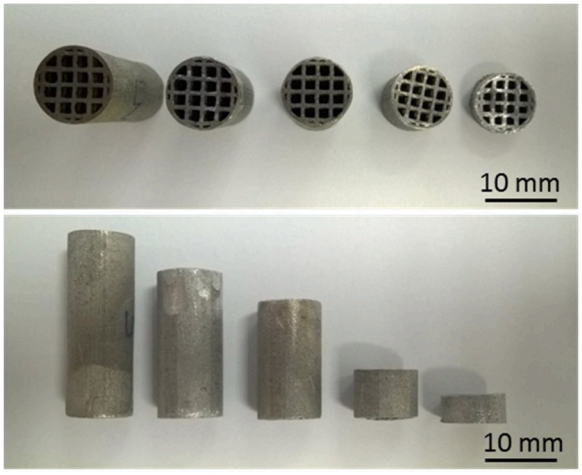

Fig. 6. Top view and side view of the 1.75 mm cell size POCS (samples F, E, D, B, A, left to right).

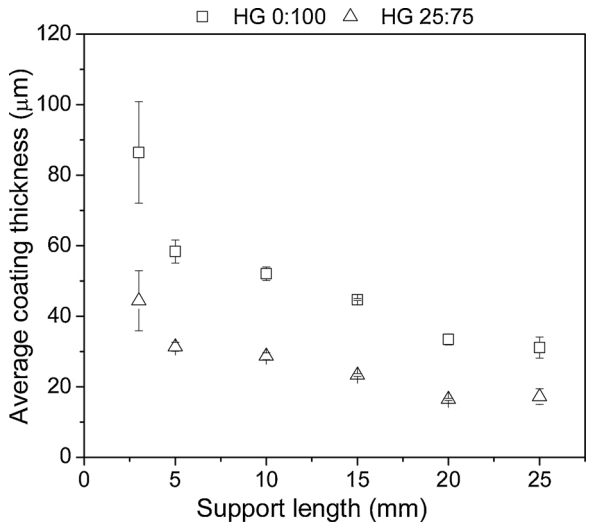

Fig. 7. Average wet coating thickness as a function of support length (b). POCS cell size and spinning speed are fixed at 1.75 mm and 2000 rpm, respectively. Error bars are the standard deviation from 3 replicate experiments.

decrease with increasing POCS length. This trend can be possibly explained by considering the centrifugal forces acting on the samples during coating deposition and the position of the sample in the rotating system. POCS are fixed to the rotating shaft with a specifically designed sample holder, which keeps the sample in horizontal position with the longitudinal axis of the POCS perpendicular to the rotation axis. The centrifugal force increases with the distance from the rotation axis and, thus, a stronger liquid drain should prevail at the edges of longer samples, if compared to shorter ones. Then, the simultaneous actions of capillarity and liquid medium continuity can induce the reported difference in liquid removal behavior. Centrifugal force (F_{CF}) is defined as

$$F_{CF} = m\omega^2 r \quad (2)$$

where m (kg) is the mass of the body, ω (rad s^{-1}) is the angular velocity and r (m) is the distance from the rotating axis. In our system layout, the POCS is fixed to the rotating axis by a sample holder; thus, the mass of the POCS should not be considered in the evaluation of centrifugal forces acting on the fluid. As additional hypothesis, the mass of the liquid that is entrapped inside the POCS porosity will not be taken into consideration. This is a strong simplification when samples of different length are considered, as each one of them will entrap a different mass of liquid before spinning. Despite that, it should be considered that the liquid mass per unit volume is constant, as far as cell density, geometrical properties and liquid composition are fixed. Considering the layout of the device, POCS are placed horizontally in the sample holder with the longitudinal axis perpendicular to the rotation axis of the device; the center of mass of the support is in correspondence of the axis of rotation of the device. The maximum distance from the rotation axis (r) is equal to half of the POCS length. Thus, the influence of the centrifugal acceleration (ωr) on average coating thickness was investigated, both using POCS of different length (Fig. 6) and varying the angular velocity (Fig. 8).

Average coating thickness decreases with the increase of centrifugal acceleration, which acts as the main driving force during the excess slurry removal from POCS structures. These results are also in accordance with data shown in Fig. 7, corroborating the idea that longer samples are exposed to stronger excess liquid removal, thus resulting, at fixed liquid medium composition, in thinner wet coating layers onto the POCS surface.

In order to further assess the influence of POCS geometric parameters on wet coating deposition, samples with different specific surface area (S_v) were tested. As reported in Table 1 and by Klummp et al. [20], the

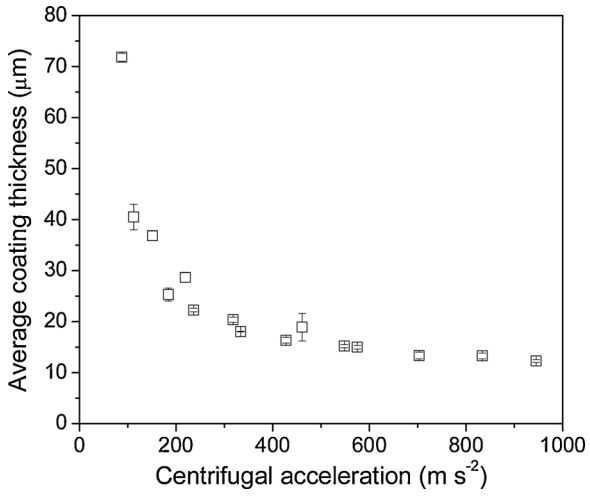

Fig. 8. Average wet coating thickness as a function of centrifugal acceleration for 1.75 mm cell size POCS of different length using a 75 %wt. glycerol solution. Error bars are the standard deviation from 3 replicate experiments.

surface area of these structures is a function of the cell size, of the porosity and of the strut diameter. Moreover, it represents the available surface to be covered by the liquid medium and therefore in our opinion it represents the controlling parameter to characterize the loading and the coating thickness.

On the other hand, due to the dependences listed above, it is impossible to change one of the other parameters while keeping the same surface area. In Fig. 9 the average coating thickness and the average coating load are reported as a function of S_v.

At any liquid medium viscosity, the average wet coating thickness is nearly constant upon varying S_v (Fig. 9-a). Reported results are consistent with the equilibrium between the forces acting on the liquid medium during the spin coating process, namely the driving force of liquid removal (i.e. the centrifugal force) and the viscous force, which opposes to entrapped liquid removal. Given the proportionality of both forces to S_v, the average wet coating thickness resulted independent of the specific surface area. Given the constancy of the wet coating thickness at fixed liquid medium viscosity, the average wet coating load per unit volume increased proportionally to S_v (Fig. 9-b), as all tested samples shared similar geometric properties (i.e. sample length and diameter) and, thus, overall volumes.

3.2. POCS catalytic activation

All the samples used for catalytic activation were characterized by an external skin, which lead to different considerations for mass transfer while sample I was cut from a bigger sample, so it was tested without external skin. This additional sample was added to the experimental campaign to extend the validity of the correlation to highly porous structures and verify the effect of the skin on the mass transfer properties.

A detailed description of the preparation and characterization of the Pd/CeO_2 catalyst was reported in a previous work [17]. The catalytic powder was dispersed in the liquid medium according to the procedure reported in section 2.2 and, thus, it was used to activate POCS by slurry coating using the dip-spin coating process. Results of PdCeHS slurry deposition are presented in Fig. 10.

The slurry viscosity was measured according to the procedure reported in Section 2.2. PdCeHS slurry was found to have a slightly non Newtonian behavior in the 0.1-1000 s^{-1} range. Considering 100 s^{-1} as a representative condition of the stresses induced on the fluid during spin coating procedure, the catalytic slurry viscosity was found to be equal to 0.056 Pa s. This value was used in order to add the average wet coating load for PdCeHS slurry to the results obtained for model glycerol solutions (Fig. 10-a). Results show that the catalytic slurry fits the trend that was obtained with model glycerol solutions. Additionally, the dependence of washcoat load after flash drying on the deposition number was investigated; results are shown in Fig. 10-b. In this case, the washcoat load was found to increase linearly with the deposition number. Moreover, an increase in cell size determined a decrease in terms of deposited washcoat load. This is in accordance with results reported in Fig. 9 for wet coating load.

Washcoated samples were characterized by optical microscopy. Results are given in Fig. 11.

In all cases, good surface coverage and washcoat homogeneity is present. Thanks to the high stresses induced during spin treatment and to the high efficiency in entrapped liquid removal, no cell clogging is manifest after calcination. This is of paramount importance, in order to avoid losses during catalytic tests, which may affect catalytic performance.

Additionally, samples with 1.5 and 2.25 mm cell sizes have been used to measure the washcoat thickness, according to the procedure of Section 2.2. Once support porosity was filled with resin, samples were cross sectioned after curing by cutting along the axial direction. Then, samples were polished on both sides and a characterization of internal surfaces was thus possible. Different degrees of polishing were

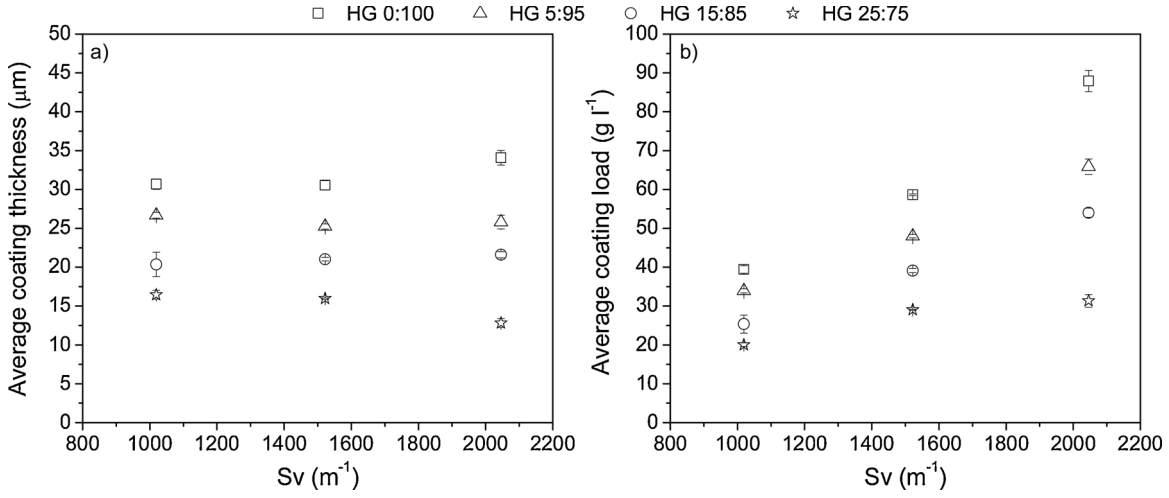

Fig. 9. Influence of specific surface area (S_v) on average wet coating thickness (a) and load (b) for different liquid media. Rotation speed and time are fixed at 2000 rpm and 90 s, respectively. Error bars are the standard deviation from 3 replicate experiments.

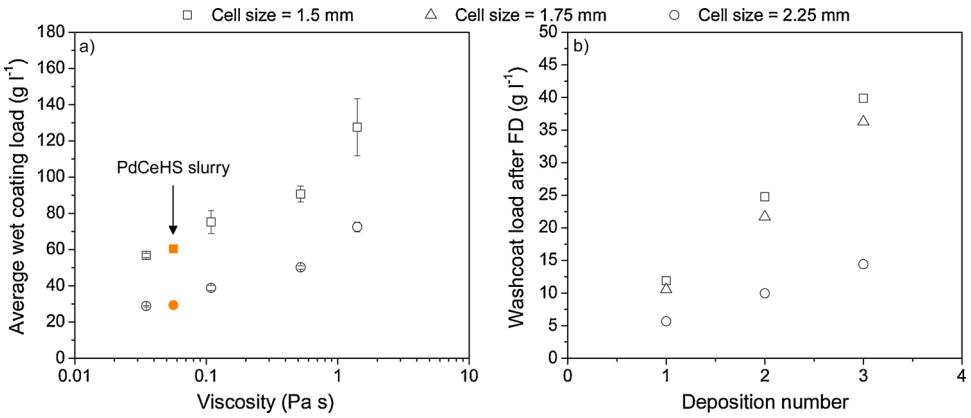

Fig. 10. Average wet coating load as a function of liquid media viscosity (a, black empty symbols refer to water-glycerol model solutions, orange full symbols refer to the catalytic slurry) and solid washcoat load after flash drying as a function of deposition number (b). Rotation speed was set at 2000 rpm, while rotation time was set at 10 s.

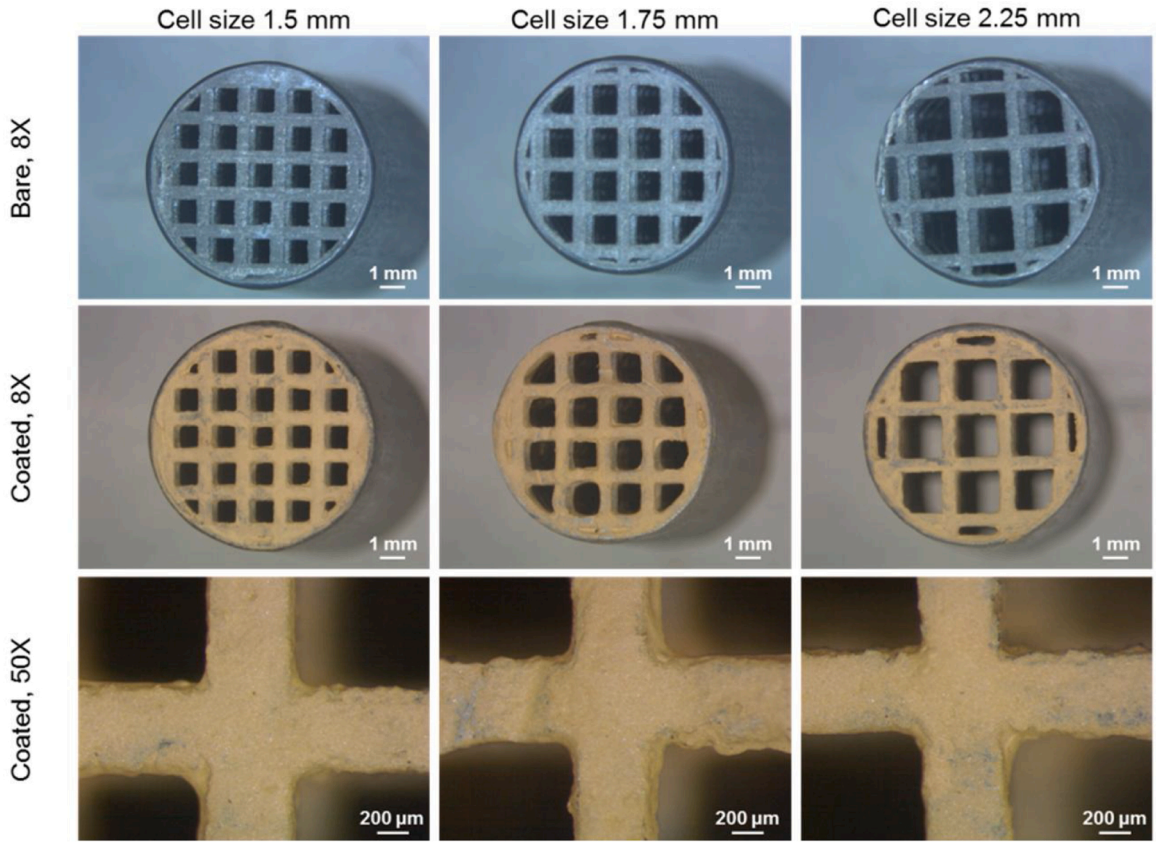

Fig. 11. Optical microscope analysis in cross section view of POCS with 1.5 (left column), 1.75 (central column) and 2.25 mm (right column) cell sizes: bare supports (first row) and samples at 8X (second row) and 50X magnification (third row).

performed on the two parts of the same sample, aiming at investigating a large variety of cross sections.

Results of optical microscope analysis, shown in Fig. 12, confirm the presence of an apparently homogeneous layer on the POCS surface. In cross-sectional view, washcoat thickness appears to be not uniform due to the lack of homogeneity of the support material: a washcoat thickness in the range of 10−20 µm was in fact measured.

3.3. Catalytic CO oxidation tests

To demonstrate the potential of these structures as catalyst supports, CO oxidation in air was chosen as reference reaction for environmental applications. First, blank tests were performed loading bare samples and feeding a flow rate of 1000 cm^3 min^{-1} STP from room temperature up to an oven temperature of 500 °C; the conversion of the system was lower than 5%, as expected the uncoated POCS and the reactor were not active for the CO oxidation. Then, the absence of preferential gas-pathways (bypass) and the evaluation of the catalyst activity were checked by performing tests at 1000 cm^3 min^{-1} STP; in this case, conversions higher than 99 % were recorded. Hence, catalytic tests on different supports and at different flow rates were performed. Fig. 13 shows the light-off curves collected over the POCS with d_{cell} equal to 1.75 mm and 1.5 mm at flow rates of 3000 and 6000 cm^3 min^{-1} STP, respectively, which correspond to flow velocities close to 1 and 2 m s^{-1} at standard

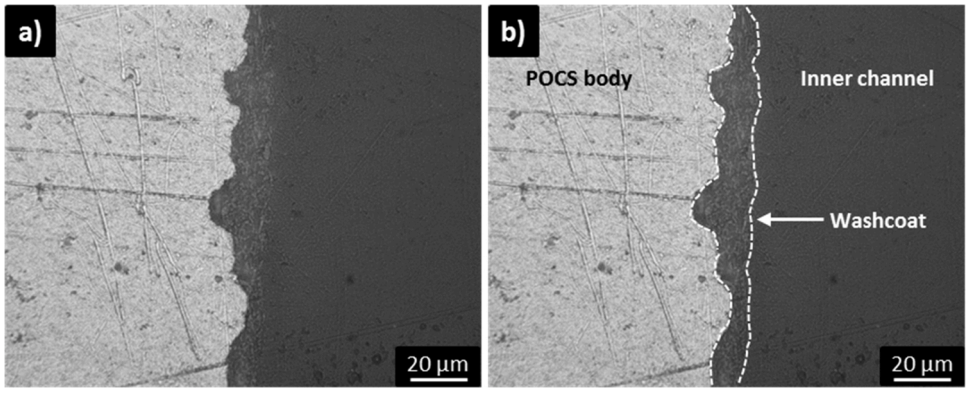

Fig. 12. Optical microscope analysis of a cross-sectioned POCS of 1.75 mm cell size (a) and same picture with image processing (b).

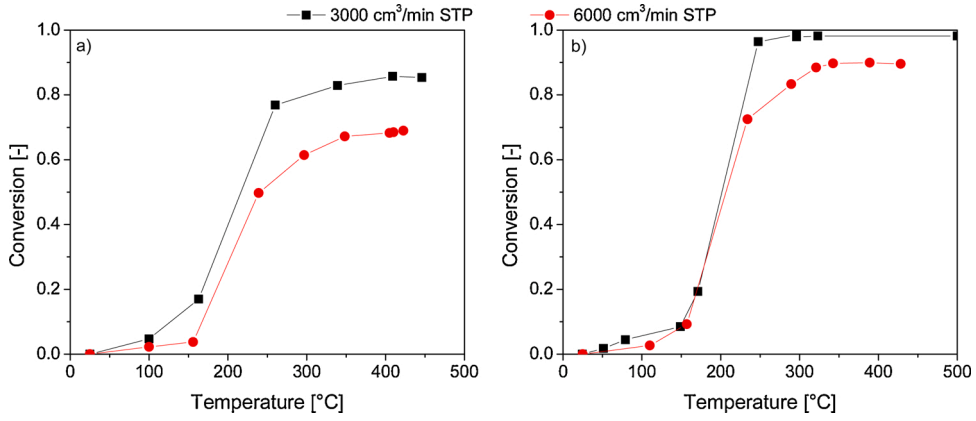

Fig. 13. Light-off curves at different flow rates for supports with 1.75 mm (a) and 1.5 mm (b) cell size.

conditions. The curves show a similar behavior: a lower catalytic activity was present for temperatures lower than 100 °C, then the conversion increases rapidly, alongside with an increase of the temperature in the system, due to the exothermal extent of the reaction. Afterwards, at temperatures around 250−300 °C the dependency of the conversion on the temperature becomes much lower, a characteristic feature of the transition between chemical and external mass transfer regime. Despite the short residence time, the CO conversion achieved with these supports in the diffusion-limited regime is remarkably high, revealing the potential of these structures to act as enhanced catalyst supports for diffusion-limited gas/solid applications. The conversion of the support with higher cell density is higher both because of the higher exposed area and due to an increased mass transfer rate, as it will be elucidated in the next paragraph. In both the supports, light-off was reached below 150 °C for the tested flow rates.

3.4. Evaluation of mass transfer rates

Conversions in mass transfer regime collected for the investigated samples with different flow rates and feed composition were analyzed according to the classical dimensionless approach.

The volumetric mass transfer coefficient k_v was calculated as reported in Eq. (3).

$$k_v = \frac{-\ln(1-\eta)}{\tau} \tag{3}$$

where η is the conversion and τ is the residence time, defined as L/v. As expected, the volumetric mass transfer coefficients increase on increasing both the flow velocity and the cell density of the substrate as well as when switching to He as a diluting gas.

Due to the manufacturing techniques described in the previous section, samples are characterized by a skin, which improves the mechanical resistance of the structure. In the coating process, the whole surface of the sample, including the inner skin surface is coated; therefore, also this surface, whose area corresponds up to 20 % of the whole active one, contributes to the conversion of the limiting species (CO).

In order to find a correlation for mass transport in idealized and infinite cubic POCS, we attempted to remove the impact of the skin internal surface on the overall conversion. Since the samples are circular, we assumed that such surface can be characterized by the same mass transfer properties of a circular channel with the inner diameter and the same surface area. Since the flow is already developed and laminar in the tube ($Re_{tube\ max} < 900$), only the asymptotic contribution was considered.

$$k_{v,tube} = k_{m,tube} S_{v,skin} = \frac{Sh_{tube} D_{CO,Mix}}{d_{tube}} S_{v,skin} \tag{4}$$

$$Sh_{tube} = 3.66 \tag{5}$$

The volumetric mass transfer coefficient of POCS was then calculated as

$$k_{v,POCS} = k_v - k_{v,tube} \tag{6}$$

The mass transfer coefficient k_m was then calculated with the following expression:

$$k_{m,POCS} = k_{v,POCS} / S_{v,POCS} \tag{7}$$

To assess the accuracy of this approximation, an additional sample (sample I) was prepared without external skin by cutting a bigger structure using the waterjet technique. This eliminates the spurious

contribution of the additional active surface, thus making the evaluation of the mass transfer coefficient of the POCS lattice straightforward.

In analogy with open cell foams [33], which closely resemble the POCSs structure, the strut diameter was chosen as the characteristic length for a dimensionless analysis. The Sherwood number and the Reynolds numbers for these structures were therefore calculated as in Eq.s 8–10:

$$Sh_{ds} = \frac{k_{m,POCS} D_{CO,mix}}{d_s} \quad (8)$$

$$\mathrm{Re}_{ds} = \frac{\rho u d_s}{\mu} \quad (9)$$

$$\mathrm{Sc} = \frac{\mu}{\rho D_{CO,mix}} \quad (10)$$

From the $\mathrm{ShSc}^{1/3}$ vs Re data plot in Fig. 14-a, some effects are evident. The data at low Reynolds collected in helium display a lower slope than all the other data collected at $\mathrm{Re} > 10$. This is in analogy with recent literature on mass transport in open cell foams [33] and in fibrous media [35]. The Sh data in this regime display a slope close to 1/3, as proposed by Ishimi et al. [36] for tube banks. The increase of the mean slope is instead associated with the onset of dissipative phenomena that enhance the mass transport. To match this change in the slope, in analogy with foams, it is possible to consider the superposition of the two behaviors expected in these structures, namely the laminar flow regime, with Sh depending on $\mathrm{Re}^{1/3}$, and the dissipative regime characterized by a dependence of Sh on $\mathrm{Re}^{0.8}$. From Fig. 14 a) it is also possible to notice the effect of porosity on the dimensionless mass transfer coefficients. On decreasing the porosity of the structure, the Sh number increases, in line with correlations for external mass transfer in other catalyst supports (foams, packed beds) and for heat transfer in tube bundles. A linear inverse dependence on the void fraction (ε^{-1}) is found here in the case of square-channelled POCS, like reported for heat transfer to tube banks and in contrast with the -2 exponent reported for foams in [33]. By numerical regression, the correlation of Eq.11 was derived. A good agreement with the collected experimental data is noted, as documented in Fig. 14-b.

$$Sh = \varepsilon^{-1}(0.29\mathrm{Re}^{0.33} + 0.032\mathrm{Re}^{0.8})Sc^{1/3} \quad (11)$$

To better understand the potential of these structures as enhanced substrates for mass transfer limited catalytic processes, volumetric mass transfer coefficients are calculated and compared with those of state of the art honeycombs. CO oxidation in air at 573 K and ambient pressure is considered as a representative environmental application. Flow velocities in the range (1—15) $\mathrm{m{\cdot}s^{-1}}$ are investigated corresponding to typical conditions in exhaust aftertreatment devices for mobile applications (i.e. Gas Hourly Space Velocities in the range $24000-360000\,\mathrm{h^{-1}}$). Two square channel honeycombs, the 600 Channels Per Square Inch (CPSI) 3.5 mils[2] and the 900 CPSI 2.5 mils honeycombs are used as benchmark for comparison assuming fully developed laminar flow conditions (Sh HC = 2.997). Cubic cell POCS with strut size equal to 0.5 mm and 0.2 mm are considered respectively. By using investment casting and Selective Laser Melting (SLM) [37] it is possible to print lattice structures with struts of 0.5 – 0.6 mm, as reported in this work. On the other hand, with ceramic stereolithography, it is possible to print samples with much higher detail, with dimension of 0.2 mm as reported by Santoliquido et al. [38]. Void fractions varying in the range (0.80 – 0.90) are chosen in line with typical values of OFA in commercial honeycombs. Table 3 reports the geometrical features of these samples. Fig. 15 shows the performances of these catalyst supports. A different dependency of k_v on the flow rate (constant k_v for honeycombs, increasing k_v for POCS) is observed coherently with the different flow field inside these structures. However, it is evident that structures with strut size of 0.5 mm present quite low volumetric mass transfer rates with respect to the commercial honeycombs, while cubic POCS with struts of 0.2 mm show mass transfer rates in the same range ($\varepsilon = 0.9$) or higher than the considered honeycombs ($\varepsilon = 0.8-0.85$). These results highlight the potential of these materials to act as enhanced catalyst carrier for environmental applications.

Technological developments of additive manufacturing techniques able to produce structures with thinner struts would provide increasing advantages. Besides recent numerical studies [19] highlighted that the POCS cell shape has strong effects on the mass transfer rates, showing in particular that other cell geometries present better mass transfer rates with respect to the simple cubic geometry. Finally, it is worth to remark that pressure drop performances need to be assessed for a more comprehensive evaluation of the potential of POCS structures in environmental applications.

4. Conclusions

We have systematically investigated the preparation and the properties of novel structured catalysts for environmental applications, whose substrates are periodic open cellular structures (POCS) conveniently manufactured by investment casting and catalytically activated by washcoating.

Model liquids based on water-glycerol mixtures were effectively used to mimic the behavior of the catalytic slurry in the washcoating of POCS. Accordingly, fundamental knowledge concerning wet coating layer deposition and management on POCS could be collected. In particular, the effects of spinning speed, spinning time, liquid media viscosity and support geometrical properties (i.e. cell size and support length) on coating deposition were studied. The coating load was found to decrease with the increase of spinning speed and time: promising results were obtained in terms of control of the wet coating thickness.

Based on these results, POCSs were effectively activated by depositing Pd/CeO_2 catalyst by slurry coating, using a dip-coating/spin-coating mixed procedure. Homogeneous catalytic layers were characterized by optical microscope and samples were tested in the CO oxidation. Good results were obtained in terms of CO conversion and stability of the catalytic performances at industrially relevant space velocities. On the basis of the results herein collected, we developed a mass transfer correlation for cubic-cell POCS. The mass transfer correlation was used to compare the performances of these structures in terms of volumetric mass transfer coefficients k_v. The tested geometries present struts with dimensions of 0.5 mm. Considering structures with porosities in the range (0.8–0.9) this leads to poor surface to volume ratios and volumetric mass transfer coefficients. However, novel 3D printing techniques (e.g. stereolithography) enable the design of supports with smaller strut size in the range 0.2 mm. With these structures, significantly higher volumetric mass transfer coefficients are expected, comparable or higher than for state of the art honeycomb supports. Further studies will address the optimization of the cell shape of the POCS to increase the volumetric mass transfer rates and to overcome the current technological limit represented by honeycombs, as well as to assess the pressure drop performances of POCS.

CRediT authorship contribution statement

Riccardo Balzarotti: Data curation, Methodology, Investigation, Validation, Formal analysis, Visualization, Writing - original draft. **Matteo Ambrosetti:** Data curation, Methodology, Investigation, Validation, Formal analysis, Visualization, Writing - original draft. **Mauro Arnesano:** Investigation, Methodology, Writing - original draft. **Alfredo Anglani:** Conceptualization, Investigation, Methodology, Writing - review & editing. **Gianpiero Groppi:** Conceptualization, Methodology, Resources, Writing - review & editing, Supervision. **Enrico Tronconi:** Conceptualization, Resources, Writing - review & editing, Supervision,

[2] One thousandth of an inch (2.54 μm)

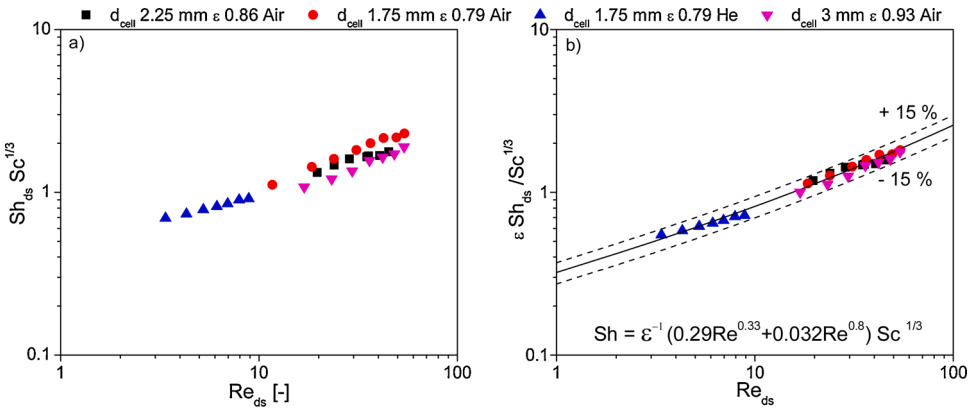

Fig. 14. Experimental dimensionless mass transfer coefficients for square channel POCS (a) and comparison between experimental data and proposed correlation for mass transfer in square cell POCS (b).

Table 3
Geometrical properties of POCS and honeycombs used for evaluation in Fig. 15.

POCS					Honeycomb				
Name	ds [μm]	ε [-]	d_{cell} [mm]	S_v [m^{-1}]	Name	Wall thickness [μm]	OFA [-]	dh [mm]	S_v [m^{-1}]
A	500	0.90	2.55	741	HC 600 3.5	89	0.835	1.036	3224
B	500	0.85	2.05	1081	HC 900 2.5	64	0.855	0.847	4042
C	500	0.80	1.74	1412					
D	200	0.90	1.02	1852					
E	200	0.85	0.82	2703					
F	200	0.80	0.696	3530					

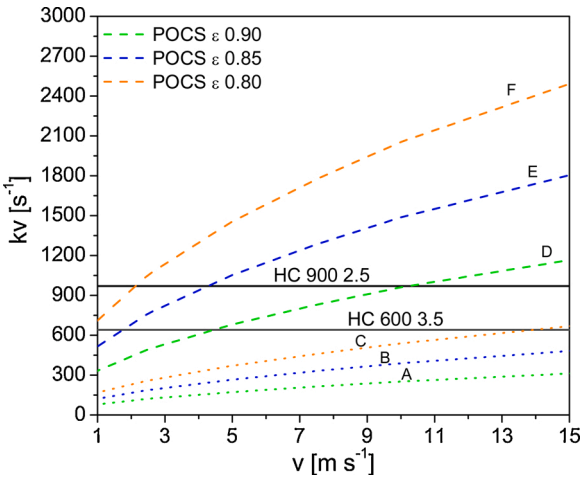

Fig. 15. Evaluation of volumetric mass transfer coefficients of different supports: solid lines = honeycombs, dotted lines POCS with d_s 0.5 mm, dashed lines POCS with d_s 0.2 mm.

Project administration, Funding acquisition.

Declaration of Competing Interest

The authors report no declarations of interest.

Acknowledgments

The research leading to these results has received funding from the European Research Council under the European Union's Horizon 2020 Research and Innovation Program (Grant Agreement no. 694910/ INTENT: "Structured Reactors with Intensified Energy Transfer for Breakthrough Catalytic Technologies") and from MIUR FARE RICERCA IN ITALIA, project BEATRICS Grant R16R7NLWPW.

References

[1] A. Cybulski, J.A. Moulijn, Structured Catalysts and Reactors, second edition, 2005, https://doi.org/10.1201/9781420028003.
[2] P.H. Ho, M. Ambrosetti, G. Groppi, E. Tronconi, J. Jaroszewicz, F. Ospitali, E. Rodriguez-Castellon, G. Fornasari, A. Vaccari, P. Benito, One-step electrodeposition of Pd-CeO_2 on high pore density foams for environmental catalytic processes, Catal. Sci. Technol. 8 (2018) 4678–4689, https://doi.org/10.1039/C8CY01388H.
[3] S.T. Sie, H.P. Calis, Structured Catalysts and Reactors, CRC Press, 2005, https://doi.org/10.1201/9781420028003.
[4] E. Verlato, S. Barison, S. Cimino, F. Dergal, L. Lisi, G. Mancino, M. Musiani, L. Vàzquez-Gòmez, Catalytic partial oxidation of methane over nanosized Rh supported on Fecralloy foams, Int. J. Hydrogen Energy 39 (2014) 11473–11485, https://doi.org/10.1016/j.ijhydene.2014.05.076.
[5] J. Kryca, P.J. Jodłowski, M. Iwaniszyn, B. Gil, M. Sitarz, A. Kołodziej, T. Łojewska, J. Łojewska, Cu SSZ-13 zeolite catalyst on metallic foam support for SCR of NOx with ammonia: Catalyst layering and characterisation of active sites, Catal. Today 268 (2016) 142–149, https://doi.org/10.1016/j.cattod.2015.12.018.
[6] L. Giani, G. Groppi, E. Tronconi, Mass-transfer characterization of metallic foams as supports for structured catalysts, Ind. Eng. Chem. Res. 44 (2005) 4993–5002, https://doi.org/10.1021/ie0490886.
[7] A. Montebelli, C.G. Visconti, G. Groppi, E. Tronconi, C. Ferreira, S. Kohler, Enabling small-scale methanol synthesis reactors through the adoption of highly conductive structured catalysts, Catal. Today 215 (2013) 176–185, https://doi.org/10.1016/j.cattod.2013.02.020.
[8] D. Merino, O. Sanz, M. Montes, Effect of the thermal conductivity and catalyst layer thickness on the Fischer-Tropsch synthesis selectivity using structured catalysts, Chem. Eng. J. 327 (2017) 1033–1042, https://doi.org/10.1016/J.CEJ.2017.07.003.
[9] P.S. Roy, N.-K. Park, K. Kim, Metal foam-supported Pd–Rh catalyst for steam methane reforming and its application to SOFC fuel processing, Int. J. Hydrogen Energy 39 (2014) 4299–4310, https://doi.org/10.1016/J.IJHYDENE.2014.01.004.
[10] V. Palma, D. Pisano, M. Martino, P. Ciambelli, Structured catalysts with high thermoconductive properties for the intensification of Water Gas Shift process, Chem. Eng. J. 304 (2016) 544–551, https://doi.org/10.1016/J.CEJ.2016.06.117.
[11] G. Do, T. Stiegler, M. Fiegl, L. Adler, C. Körner, A. Bösmann, H. Freund, W. Schwieger, P. Wasserscheid, Electrophoretic deposition of boehmite on additively manufactured, interpenetrating periodic open cellular structures for catalytic applications, Ind. Eng. Chem. Res. 56 (2017) 13402–13410, https://doi.org/10.1021/acs.iecr.7b02453.
[12] A. Vita, C. Italiano, C. Fabiano, L. Pino, M. Lagana, V. Recupero, Hydrogen-rich gas production by steam reforming of n-dodecane part I: catalytic activity of Pt/CeO_2

catalysts in optimized bed configuration, Appl. Catal. B-Environ. 199 (2016) 350–360, https://doi.org/10.1016/j.apcatb.2016.06.042.
[13] C. Italiano, R. Balzarotti, A. Vita, S. Latorrata, C. Fabiano, L. Pino, C. Cristiani, Preparation of structured catalysts with Ni and Ni-Rh/CeO_2 catalytic layers for syngas production by biogas reforming processes, Catal. Today 273 (2016) 3–11, https://doi.org/10.1016/j.cattod.2016.01.037.
[14] V. Meille, Review on methods to deposit catalysts on structured surfaces, Appl. Catal. A Gen. 315 (2006) 1–17, https://doi.org/10.1016/j.apcata.2006.08.031.
[15] R. Balzarotti, C. Cristiani, S. Latorrata, A. Migliavacca, Washcoating of low surface area cerium oxide on complex geometry substrates, Part. Sci. Technol. 34 (2016) 184–193, https://doi.org/10.1080/02726351.2015.1058872.
[16] R. Balzarotti, C. Cristiani, L.F. Francis, Spin coating deposition on complex geometry substrates: Influence of operative parameters, Surf. Coat. Technol. 330 (2017) 1–9, https://doi.org/10.1016/j.surfcoat.2017.09.077.
[17] M. Ambrosetti, R. Balzarotti, C. Cristiani, G. Groppi, E. Tronconi, M. Ambrosetti, R. Balzarotti, C. Cristiani, G. Groppi, E. Tronconi, The Influence of the washcoat deposition process on high pore density open cell foams activation for CO catalytic combustion, Catalysts 8 (2018) 510, https://doi.org/10.3390/catal8110510.
[18] C. Busse, H. Freund, W. Schwieger, Intensification of heat transfer in catalytic reactors by additively manufactured periodic open cellular structures (POCS), Chem. Eng. Process. Process Intensif. 124 (2018) 199–214, https://doi.org/10.1016/j.cep.2018.01.023.
[19] V. Papetti, P. Dimopoulos Eggenschwiler, A. Della Torre, F. Lucci, A. Ortona, G. Montenegro, Additive manufactured open cell polyhedral structures as substrates for automotive catalysts, Int. J. Heat Mass Transf. 126 (2018) 1035–1047, https://doi.org/10.1016/j.ijheatmasstransfer.2018.06.061.
[20] M. Klumpp, A. Inayat, J. Schwerdtfeger, C. Körner, R.F. Singer, H. Freund, W. Schwieger, Periodic open cellular structures with ideal cubic cell geometry: effect of porosity and cell orientation on pressure drop behavior, Chem. Eng. J. 242 (2014) 364–378, https://doi.org/10.1016/j.cej.2013.12.060.
[21] T. Knorr, P. Heinl, J. Schwerdtfeger, C. Körner, R.F. Singer, B.J.M. Etzold, Process specific catalyst supports—selective electron beam melted cellular metal structures coated with microporous carbon, Chem. Eng. J. 181–182 (2012) 725–733, https://doi.org/10.1016/j.cej.2011.10.009.
[22] X. Cai, M. Wörner, H. Marschall, O. Deutschmann, Numerical study on the wettability dependent interaction of a rising bubble with a periodic open cellular structure, Catal. Today 273 (2016) 151–160, https://doi.org/10.1016/j.cattod.2016.03.053.
[23] M. Lämmermann, W. Schwieger, H. Freund, Experimental investigation of gas-liquid distribution in periodic open cellular structures as potential catalyst supports, Catal. Today 273 (2016) 161–171, https://doi.org/10.1016/j.cattod.2016.02.049.
[24] C. Hutter, D. Büchi, V. Zuber, P. Rudolf von Rohr, Heat transfer in metal foams and designed porous media, Chem. Eng. Sci. 66 (2011) 3806–3814, https://doi.org/10.1016/j.ces.2011.05.005.
[25] A. Oraib, A.R.K. Abu, R. Reza, Mechanical Properties of a New Type of Architected Interpenetrating Phase Composite Materials, Adv. Mater. Technol. 2 (n.d.) 1600235. doi:10.1002/admt.201600235.
[26] A. Anglani, M. Pacella, Logistic regression and response surface design for statistical modeling of investment casting process in metal foam production, Procedia CIRP 67 (2018) 504–509, https://doi.org/10.1016/j.procir.2017.12.252.
[27] R. Balzarotti, C. Italiano, L. Pino, C. Cristiani, A. Vita, Ni/CeO_2-thin ceramic layer depositions on ceramic monoliths for syngas production by oxy steam reforming of biogas, Fuel Process. Technol. 149 (2016), https://doi.org/10.1016/j.fuproc.2016.04.002.
[28] A. Montebelli, C.G. Visconti, G. Groppi, E. Tronconi, C. Cristiani, C. Ferreira, S. Kohler, Methods for the catalytic activation of metallic structured substrates, Catal. Sci. Technol. 4 (2014) 2846–2870, https://doi.org/10.1039/c4cy00179f.
[29] G. Groppi, C. Cristiani, L. Lietti, C. Ramella, M. Valentini, P. Forzatti, Effect of ceria on palladium supported catalysts for high temperature combustion of CH_4 under lean conditions, Catal. Today 50 (1999) 399–412, https://doi.org/10.1016/S0920-5861(98)00518-5.
[30] H. Zhang, W.J. Suszynski, K.V. Agrawal, M. Tsapatsis, S. Al Hashimi, L.F. Francis, Coating of open cell foams, Ind. Eng. Chem. Res. 51 (2012) 9250–9259, https://doi.org/10.1021/ie300266p.
[31] M. Valentini, G. Groppi, C. Cristiani, M. Levi, E. Tronconi, P. Forzatti, The deposition of γ-Al_2O_3 layers on ceramic and metallic supports for the preparation of structured catalysts, Catal. Today 69 (2001) 307–314, https://doi.org/10.1016/S0920-5861(01)00383-2.
[32] M. Bracconi, M. Ambrosetti, M. Maestri, G. Groppi, E. Tronconi, A fundamental analysis of the influence of the geometrical properties on the effective thermal conductivity of open-cell foams, Chem. Eng. Process. - Process Intensif. 129 (2018) 181–189, https://doi.org/10.1016/j.cep.2018.04.018.
[33] M. Bracconi, M. Ambrosetti, M. Maestri, G. Groppi, E. Tronconi, A fundamental investigation of gas/solid mass transfer in open-cell foams using a combined experimental and CFD approach, Chem. Eng. J. 352 (2018), https://doi.org/10.1016/j.cej.2018.07.023.
[34] A.G. Emslie, F.T. Bonner, L.G. Peck, Flow of a viscous liquid on a rotating disk, J. Appl. Phys. 29 (1958) 858–862, https://doi.org/10.1063/1.1723300.
[35] E. Reichelt, M. Jahn, Generalized correlations for mass transfer and pressure drop in fiber-based catalyst supports, Chem. Eng. J. 325 (2017) 655–664, https://doi.org/10.1016/J.CEJ.2017.05.119.
[36] K. Ishimi, S. Koroyasu, H. Hikita, Mass transfer in creeping flow past periodic arrays of cylinders, J. Chem. Eng. Japan. 20 (1987) 492–498, https://doi.org/10.1252/jcej.20.492.
[37] L. Boniotti, S. Beretta, L. Patriarca, L. Rigoni, S. Foletti, Experimental and numerical investigation on compressive fatigue strength of lattice structures of AlSi7Mg manufactured by SLM, Int. J. Fatigue 128 (2019) 105181, https://doi.org/10.1016/J.IJFATIGUE.2019.06.041.
[38] O. Santoliquido, G. Bianchi, P. Dimopoulos Eggenschwiler, A. Ortona, Additive manufacturing of periodic ceramic substrates for automotive catalyst supports, Int. J. Appl. Ceram. Technol. 14 (2017) 1164–1173, https://doi.org/10.1111/ijac.12745.